Soft Matter

Check for updates

Exploiting photopolymerization to modulate liquid crystalline network actuation†

Marco Turriani,[ab] Niccolò Cosottini, [iD] ‡[a] Neri Fuochi,[ac] Diederik S. Wiersma, [iD] [ab] Daniele Martella*[ac] and Camilla Parmeggiani [iD] *[ac]

Liquid Crystalline Networks (LCNs) are widely investigated to develop actuators, from soft robots to artificial muscles. Indeed, they can produce forces and movements in response to a plethora of external stimuli, showing kinetics up to the millisecond time-scale. One of the most explored preparation technique involves the photopolymerization of an aligned layer of reactive mesogens. Following this approach, side-chain polymers are widely described, while a detailed comparison of light-responsive LCNs with different architectures is not properly addressed. In this paper, two synthetic approaches are exploited leading to photoresponsive LCNs with different architectures. Mixed main-chain/side-chain LCNs are obtained in one-pot through a thiol–acrylate chain-transfer reaction, while main-chain LCNs are achieved by a two-step approach involving an aza-Michael addition followed by acrylate crosslinking. Comparison among the two materials highlighted the superior performances in terms of tension developed upon light-activation of the former one, showing muscle-like force production comparable to standard side-chain LCNs combined with the greater ability to contract from common main-chain LCNs.

Introduction

The development of smart soft actuators able to successfully replicate the high performance of biological muscles in terms of efficiency, robustness, speed and power is still a challenging objective in materials science and could lead to great advances in biomedicine, industry and mobility.[1–5]

Since 1981, when Finkelmann first prepared Liquid Crystalline Elastomers (LCEs),[6] these polymers have been investigated as promising materials for the fabrication of soft actuators ranging from the centimetre to the micrometric scale.[7–10] Indeed, thanks to their unique characteristics, combining the entropic elasticity of polymer networks with the orientational order and responsivity of liquid crystals, they can undergo reversible, programmable, and rapid shape changes in response to various external stimuli like temperature,[11,12] chemicals,[13,14]

electricity[15] and light.[16–18] This deformation is associated with a gradual decrease of the molecular order under stimuli application (up to the isotropic phase).[19] The same behaviour was later observed also for materials with higher glass transition temperature (T_g) and elastic modulus, thus more properly named Liquid Crystalline Networks (LCNs) that are more promising in terms of force production during the actuation.[20] LCNs can reversibly interchange between different programmed 3D shapes[21,22] and perform many soft robotic functionalities including lifting weights,[12] moving on surfaces,[23–26] swimming in liquids,[27,28] grasping and manipulating objects[29–31] or self-oscillating.[32,33] Indeed, LCNs have been proposed also for tunable photonic applications,[34,35] cell scaffolds[36,37] and smart tags.[38,39] Among the external stimuli mentioned above light is one of the most promising for the actuation due to its easily tuneable intensity, wavelength and polarisation and its precise spatial and temporal control.[18] Light-driven actuators can be controlled remotely and precisely[16] without the need to heat or change the physical–chemical conditions of the external environment (such as pH), making them particularly suitable for miniaturized devices[27] and soft robots.[23,26]

Focusing on the macromolecular architecture, LCNs can be divided into two main classes, side-chain or main-chain polymers, in which mesogens are attached as side-chains or directly inside the polymeric backbone, respectively. The macromolecular architecture is fundamental to determine the mechanical and actuation behaviour, with main-chain LCNs that exhibit higher chain anisotropy, thus leading to a greater actuation

[a] LENS (European Laboratory for Non-Linear Spectroscopy) Via Nello Carrara 1, 50019 Sesto Fiorentino (FI), Italy. E-mail: daniele.martella@unifi.it, camilla.parmeggiani@unifi.it

[b] Dipartimento di Fisica e Astronomia, University of Florence, Via Sansone 1, 50019 Sesto Fiorentino (FI), Italy

[c] Dipartimento di Chimica ''Ugo Schiff'', University of Florence, Via della Lastruccia 13, 50019 Sesto Fiorentino (FI), Italy

† Electronic supplementary information (ESI) available. See DOI: https://doi.org/10.1039/d4sm01360c

‡ Current address: Department of Chemistry, University of York, YO10 5DD, York, UK.

strain.[40] Different approaches were investigated to prepare LCNs, including hydrosilylation,[6,41] polycondensation[42] and free radical polymerisation that is often preferred due to its simplicity and the possibility of using commercially widely available acrylate and methacrylate monomers.[43] The latter methodology is generally combined with surface alignment of the monomeric mixture and opens to many advantages including one step and quick preparation, possible patterning at the microscale (by photolithographic techniques)[44,45] and integration with other materials (as a coating,[46–48] printed microelements,[49] micro- or nano-particles[50]). However, curing of classical (di-)acrylate mesogens leads to a side-chain structure while LCNs having other architectures are less investigated by surface alignment and photopolymerization. Previous attempts in this direction include the exploitation of different click reactions[51] (such as thiol–ene[52,53] and thiol–yne click reactions[54,55]) mainly leading to thermoresponsive actuators.

In this paper, we focused on the preparation and characterization of photoresponsive LCNs comparing two different preparation pathways, both involving a photopolymerization. The first class of materials was obtained in a single stage through thiol–acrylate reaction, which proceeded starting from a LC diacrylate and a dithiol either through acrylate chain-growth or thiol chain-transfer to afford a mixed architecture (side-chain/main-chain) of the final system.[56–58] The second class of materials was obtained through a two-step approach involving an aza-Michael addition followed by a photocuring process, leading to main-chain polymers. Aza-Michael addition has already been used for the synthesis of LCNs starting from diacrylate liquid crystalline monomers and it is characterised by mild conditions, suitable kinetics, and high conversions.[59,60] The mechanism involves the nucleophilic attack of a primary amine, that acts as a chain extender in the polymer, at the β carbon of an α, β-unsaturated carbonyl compound.[51,61] For both approaches, the surface alignment technique was successfully achieved and the comparison of the two classes of materials (in terms of mechanical properties and behaviour as actuators) led to the identification of the thiol-derived materials as superior for the realisation of photoresponsive actuators.

Experimental

Materials

2-Methyl-1,4-phenylene bis(4-(3-(acryloyloxy)propoxy)benzoate) (RM257) was purchased from Synthon Chemicals. 1,4-Benzenedimethanethiol (BDMT), methylhydroxyquinone (MHQ), Irgacure 369, 1-dodecylamine (1-DA), dichloromethane, and 2-[N-ethyl-4-[(4-nitrophenyl)diazenyl]anilino]ethyl prop-2-enoate also known as Disperse Red 1 acrylate (DR1-A) were purchased from Merck. All the chemicals were used as received without further purification. A detailed description of the polymer preparation is reported in the ESI.†

Material characterization

Attenuated total reflectance infrared spectra (ATR-IR) were recorded using a PerkinElmer Spectrum Two, while proton nuclear magnetic resonance (1H-NMR) spectra were obtained through a Varian INOVA-400. The LC textures were observed through a Polarised Light Microscope (POM, Zeiss Axio Observer A1) in the cross-polarized mode, equipped with a Linkam PE120 hot stage and an Axio camera. The order parameter was evaluated through a custom set-up obtained by equipping the POM with a photodiode (Thorlabs S120VC), a power metre (Thorlabs PM101) and a LED lamp (Thorlabs M470L5). The thermal contraction under free-standing conditions was evaluated through optical images of films on a hot-stage (Mettler Toledo HS82) heating from 25 °C to 205 °C with a ramp of 10 °C min^{-1}. The length of the samples was recorded every 10 °C using a Pentax K500 camera equipped with a Pentax SMC 18–55 mm f 3.5–5.6 AL objective, and each picture was analysed using the ImageJ software. The storage moduli and the glass transition temperatures were evaluated through Dynamic Mechanical Analysis (DMA, PerkinElmer DMA 8000). The measures were performed in tension geometry on specimens of 4×2 mm^2, at 1 Hz frequency, 0.25% strain and an applied preload of 0.5 N. For each composition, three independent samples were analyzed. The temperature was increased from −20 °C to 90 °C with a heating rate of 3 °C min^{-1}. Tension developed under thermal actuation was evaluated through DMA. The tension developed under illumination by the LCNs was recorded in a custom-made setup[43] as described in detail in the ESI.†

Results and discussion

LCN fabrication

Photoresponsive LCNs were prepared as thin polymeric films starting from a mixture of a reactive mesogen and a comonomer (bearing amine or thiol groups) and employing the molecular alignment imposed by surface anchoring.[43] In all cases, the materials have been prepared with a homogeneous planar alignment, which leads to contraction along the rubbing direction with the maximisation of the force produced.

The first class of materials was synthesised through a single-step procedure. Briefly, the commercial mesogenic diacrylate RM257 (1 equiv.) was mixed with the dithiol chain transfer agent 1,4-benzenedimethanethiol (BDMT) and the dye DR1-A (1% mol/mol). To initiate the photopolymerization, Irgacure 369 (1% mol/mol) was chosen, while the radical scavenger methylhydroquinone (1% mol/mol) was added to avoid the thermal radical polymerization during the heating of the mixture (needed to properly mix all the components and infiltrate the mixture in the alignment cell). The amount of BDMT was varied from 0.50 to 0.75 equivalents and the materials obtained were named, respectively, LCN-SH50 and LCN-SH75 (the number indicating the dithiol equivalent content, e.g. LCN-SH50 contains 0.5 equivalent of thiols with respect to the acrylate groups, Table 1).

The mesomorphic properties of the reactive mixtures were first analysed through POM during both heating and cooling cycles. The mixtures showed birefringence and Schlieren
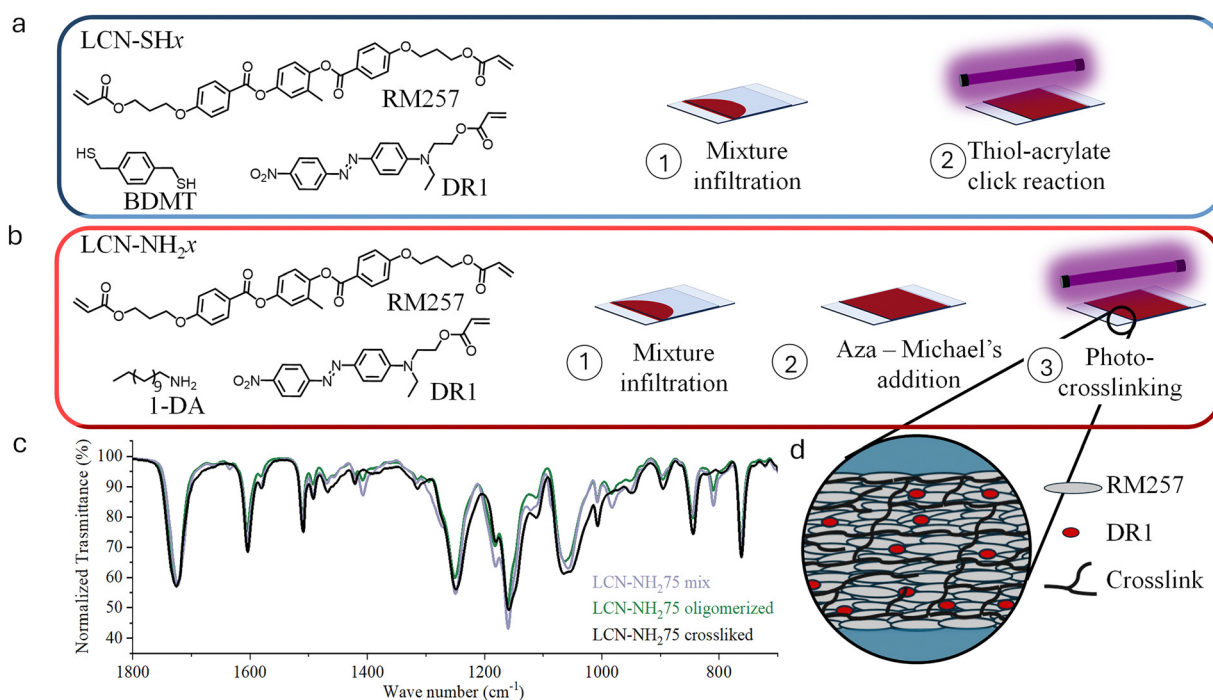
Table 1 Temperature of nematic to isotropic transition (T_{ni}) for the monomer mixtures and the oligomers measured by POM

	Equivalents BDMT	Equivalents 1-DA	T_{ni} mixture (°C)	T_{ni} oligomers (°C)
LCN-SH75	0.75		75	
LCN-SH50	0.5		105	
LCN-NH$_2$75		0.75	62	56
LCN-NH$_2$50		0.5	92	86

textures with twofold and fourfold brushes typical of the nematic mesophase (Fig. S1, ESI†). The nematic to isotropic transition temperature (T_{ni}), reported in Table 1, was consistently higher for LCN-SH50 (105 °C) with respect to LCN-SH75 (75 °C) according to the lower content in non-mesogenic comonomers. To obtain homogeneous planar aligned films, the mixtures were infiltrated by capillarity into liquid crystal cells (Fig. 1a) constituted by two microscope glass slides opportunely coated with a rubbed PVA layer.[43] The mixtures were heated above their T_{ni} before being infiltered, then the filled cells were slowly cooled to room temperature allowing for the alignment of the mesogens along the rubbing direction. The cells have been photopolymerized by UV light and the success of the process was verified through IR-ATR (Fig. S2, ESI†) observing the disappearance of the band at 1410 cm^{-1} relative to the C=C double bond of the acrylate groups and the characteristic band relative to =CH$_2$ (811 cm^{-1}). The photopolymerization did not lead to complete conversion of the acrylate group possibly due to a gel effect and a conversion of about

70–75% for both materials was estimated by ATR spectra. The thickness of the films prepared was 20 ± 4 μm for LCN-SH50 and 17 ± 3 μm for LCN-SH75.

The second class of LCNs was obtained through a two-stage approach. RM257 (1 equiv.) was mixed with DR1-A (1% mol/mol) and Irgacure 369 (2.5% weight/weight), then 1-dodecylamine was added (0.50 or 0.75 equiv.). Such mixtures were heated to be in their isotropic phase, infiltrated in liquid crystal cells, and cooled down at 50 °C (in their nematic phase) for 20 hours to obtain acrylate terminated oligomers through Michael's addition. The oligomerized mixtures were analysed by ^{1}H-NMR (Fig. S3, ESI†) to determine the RM257 conversion and the average number of LC units present in the oligomers, which were 2 and 3 for the oligomers obtained by adding 0.5 and 0.75 equivalent of 1-dodecylamine, respectively. T_{ni} was evaluated for both the reagents mixtures and the oligomers by POM (Table 1). As already noticed for the thiol base LCNs, T_{ni} was higher for the mixture with the higher concentration of mesogenic monomer (obtained by adding 0.5 equivalent of 1-dodecylamine). Furthermore, in the oligomers T_{ni} was lower if compared with the corresponding unreacted mixtures, suggesting that the oligomerization partially disturbs the order of the system. The oligomers were then cured through free radical photopolymerization by shining UV light on the cells, leading to materials named LCN-NH$_2$50 and LCN-NH$_2$75 (with respect to the amount of amine added in the first step). ATR analysis (Fig. 1b) was used to confirm the consumption of the diacrylate monomer. The thickness of the films prepared was 15 ± 4 μm for LCN-NH$_2$50 and 18 ± 4 μm for LCN-NH$_2$75.

Fig. 1 Synthesis of LCNs. (a) Representation of the principal steps for the preparation of LCN-SHx and (b) LCN-NH$_2$x. (c) ATR spectra of LCN-NH$_2$75 mixtures, LCN-NH$_2$75 after Michael's oligomerization and LCN-NH$_2$75 after photo-crosslinking reaction. (d) Representation of LCN structure at the molecular level.

Mechanical tests and order parameter evaluation.

A first qualitative assessment of the homogeneity and alignment of the films was obtained by POM observing the changes in transmittance when the sample was rotated with respect to the polarisers. In films with a good planar alignment, light extinction was observed when the director of the film was orthogonal to the polariser and the maximum transmittance when it formed a 45° angle with both the polarisers (Fig. 2a and b). For a more detailed comparison, the alignment degree of the materials was evaluated by calculating an order parameter (S) starting from the dichroic absorption (as described in ESI†) and reported in Table 2. Both thiol-based LCNs, namely LCN-SH50 and LCN-SH75, present the same order parameter ($S = 0.4$), higher than those of amino-based LCNs ($S = 0.29$ for LCN-NH$_2$50 and $S = 0.27$ for LCN-NH$_2$75). Then, the

Table 2 Order parameter and thermomechanical behaviours obtained through DMA of LCNs

	S	T_g^a (°C)	E'_{glassy} (MPa)^b	$E'_{rubbery}$ (MPa)^c	ν_c (mmol cm^{-3})
LCN-SH75	0.40	38 ± 1	4142 ± 101	8 ± 0.3	0.87 ± 0.03
LCN-SH50	0.40	35 ± 2	5246 ± 220	18 ± 5	2.08 ± 0.56
LCN-NH$_2$75	0.27	24 ± 1	1915 ± 315	4 ± 1	0.45 ± 0.11
LCN-NH$_2$50	0.29	44 ± 2	2868 ± 527	24 ± 3	2.8 ± 0.33

^{a} Defined as the temperature corresponding to the maximum of tan(δ) curves. ^{b} Storage modulus (E') 40 °C below T_g. ^{c} Storage modulus (E') 50 °C above T_g.

thermomechanical properties of the materials were investigated through DMA. Fig. 2c reports the storage modulus (E') and tan(δ) representative curves of all samples, showing for all of them three different regions in the storage modulus traces: a glassy plateau at low temperatures followed by a jump of 2–3 orders of magnitude in correspondence of the glass transition temperature, and by a second plateau at high temperatures corresponding to a rubbery plateau. LCN-SH50 and LCN-SH75 showed a sharper transition, and therefore narrower tan(δ) curves, and higher E' values in the glassy state than LCN-NH$_2$50 and LCN-NH$_2$75 (Table 2). From the storage modulus (E') value in the rubbery plateau, the crosslinking density (ν_c) of all samples was also estimated,[62] showing how, as expected, material composition is the leading factor in its modulation (Table 2). Indeed, samples obtained by different synthetic approaches but with the same ratio between the two co-monomers present similar ν_c values (LCN-NH$_2$50 vs. LCN-SH50 and LCN-NH$_2$75 vs. LCN-SH75), while changing the ratio between the two co-monomers induce a ν_c increase of six times for the amino-based materials (LCN-NH$_2$75 vs. LCN-NH$_2$50) and of about three times for the thiol-based materials (LCN-SH75 vs. LCN-SH50). In line with these results, the glass transition T_g, obtained as the maximum of the tan(δ) curve, was consistently higher for LCN-NH$_2$50 ($T_g = 45$ °C) if compared with LCN-NH$_2$75 ($T_g = 24$ °C) as expected for a more crosslinked material. LCN-SH50 and LCN-SH75, otherwise, showed a similar T_g of, respectively, 35 °C and 38 °C.

Comparing all the materials and the mechanical data collected, we can conclude that the mechanical properties look to be more effectively modulated by the oligomerization strategies (LCN-NH$_2$x series) allowing to obtain a more pronounced differentiation in parameters as the storage modulus and T_g.

Thermal and light actuation

The actuation properties under thermal stimulation were evaluated both under free-standing and isometric conditions. Briefly, for free-standing experiments, the length of LCN strips without any load applied was measured during a heating ramp (Fig. 3a). Due to the homogenous planar alignment, the films can gradually contract along the nematic director as reported in Fig. 3b. The thiol-based LCNs reached a contraction of 36% at 205 °C, higher than both the amino-based materials (23% for LCN-NH$_2$50 and 27% for LCN-NH$_2$75) at the same temperature and in agreement with the higher level of order of these
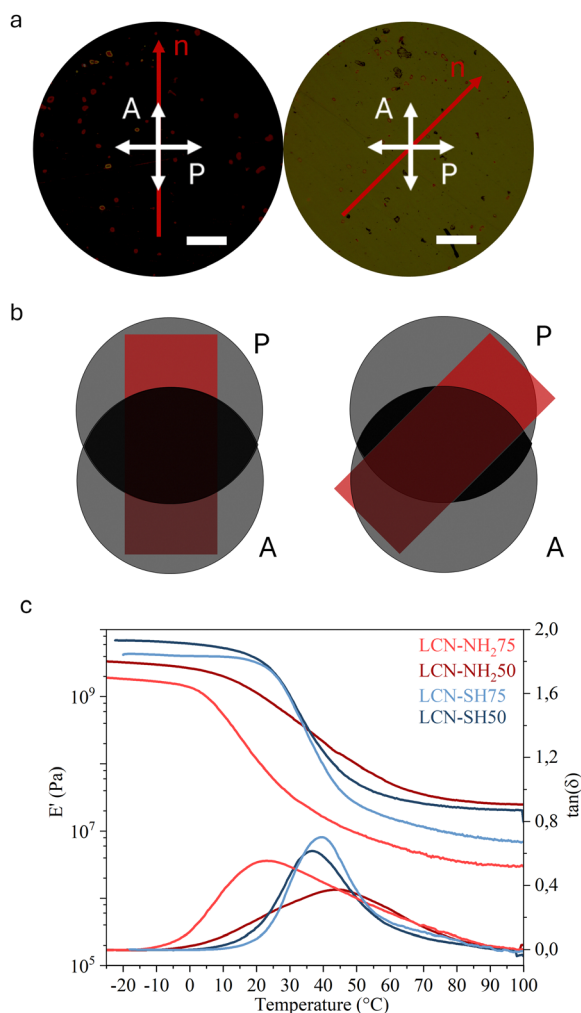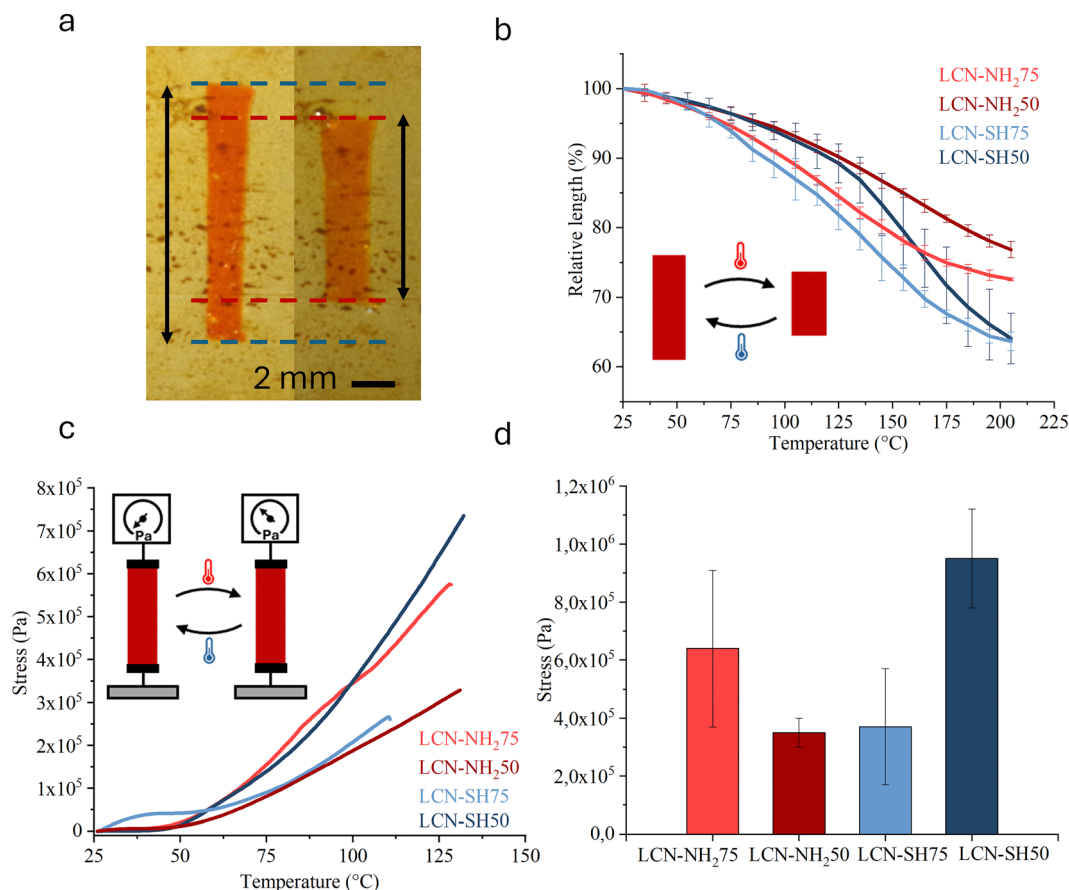

Fig. 2 Molecular alignment and mechanical tests on LCN films. (a) POM images of an LCN film with the director (n) oriented orthogonally to the polarisers and at 45°. Scale bar: 200 μm. (b) Schematization of the transmittance of LCN films under two crossed polarizer (P) and analyser (A). (c) Storage modulus (E') and tan(δ) representative curves for the LCNs synthesised.

Fig. 3 **Thermal actuation of LCNs.** (a) Picture showing the thermal actuation under free standing conditions of an LCN-NH$_2$75 sample at 25 °C (left) and 200 °C (right). (b) Thermal actuation under free standing conditions for all the LCN films. (c) Examples of one representative trace of tension *vs.* temperature for each LCN in thermal actuation experiments performed under isometric conditions. (d) Average over three measures of the maximum tension reached by each material.
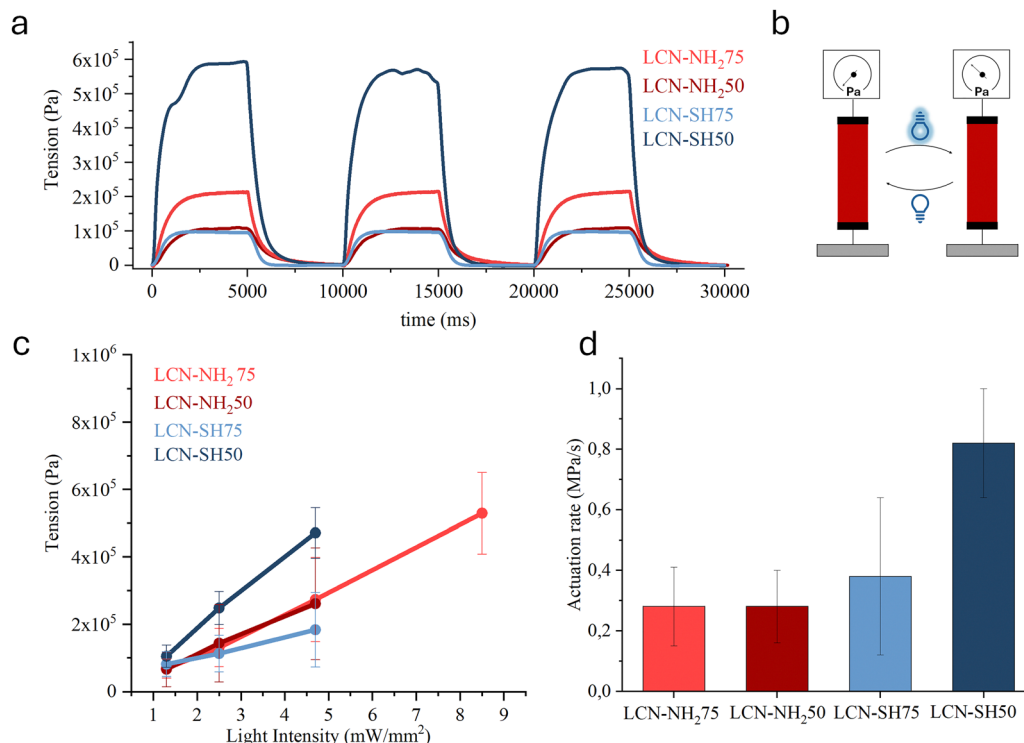
materials. It is interesting to note that the temperature to obtain the maximum rate of actuation, obtained as the minimum of the first derivative of the actuation curves, moves to higher values increasing the crosslinking density of the materials. Indeed, it passes from 124 °C for the less crosslinked material (LCN-NH$_2$75) to 165 °C for the more crosslinked ones (LCN-NH$_2$50 and LCN-SH50).

The thermal actuation analysis under isometric conditions was conducted through DMA. The sample strips, obtained by cutting LCN films along their direction, were fixed to avoid their contraction during the measurement. The tension developed was registered during a heating ramp as reported in Fig. 3c. The specimens' behaviour was similar for all the materials: after the first plateau region, the tension started to increase in a pseudo-linear way before reaching a maximum at which the samples broke. Fig. 3d shows the average over three samples of the stress at the break for each material. From the data emerges how LCN-SH50 was the material with the higher performance reaching the maximum tension developed of 0.95 MPa at 135 °C. Anyway, there was not an evident and clear correlation between the structural properties of the LCNs and the performances in terms of tension developed.

Such high actuation temperatures should be a limit, particularly for biological applications, and further studies would be needed to decrease them and to fit the requirements of the specific device to be designed, *e.g.* by playing on the mesogenic compositions.[63,64] However, thermal actuation is here presented as a way to further characterize the materials, while we believe that their photoactuation deserves to be better investigated since it involves more biocompatible and interesting temperatures (close to room temperature). The actuation behaviour of LCNs was therefore evaluated under illumination by using a custom setup (Fig. S4, ESI†).[43] In this case, the photoactuation is controlled by the azobenzene derivatives (DR1-A) bonded to the polymeric network. Under light irradiation (by blue LED with the chosen dye),[65] such photoswitches can isomerize from the *trans* to the *cis* form driving a macroscopic deformation by a photomechanical and/or photothermal mechanism.[66] When the light stimulus was switched on, the samples began to generate a mechanical tension that increased with time before reaching a plateau in approximately 1.5 seconds. When the light was switched off, the specimen relaxed completely in approximately 2 seconds.

A comparison between the materials under activation at 4.7 mW mm^{-2} is reported in Fig. 4a, the schematization of

Fig. 4 **Photo-actuation of LCNs.** (a) Traces of tension developed by LCNs during light actuation at 4.7 mW mm^{-2}. (b) Schematization of light actuation experiment. (c) Average of the maximum tension developed by the materials *vs.* intensity of light. (d) Rate of actuation of LCNs at 4.7 mW mm^{-2}, obtained as the slope of the tangent in the first 200 ms of the tension traces.

the light actuation experiment is shown in Fig. 4b, while the maximum force produced by varying the light intensity between 1.3 mW mm^{-2} and 8.5 mW mm^{-2} is shown in Fig. 4c. In this range, the maximum tension generated by the LCNs (taken in the plateau region of the force trace) increases in a pseudo-linear way with the light intensity, then reaches a threshold in which the sample breaks (Fig. 4c). LCN-SH50 and LCN-SH75 exhibit, respectively, the higher and the lower efficiency, understood as the ratio between developed tension and light intensity: the more crosslinked one (LCN-SH50) reached a maximum tension of 0.47 MPa at 4.7 mW mm^{-2}, while LCN-SH75 could develop 0.18 MPa at the same light intensity. The two amino-based LCNs showed similar behaviour in terms of efficiency but LCN-NH$_2$75 could withstand higher light intensities, up to a value of 8.5 mW mm^{-2}, without break and reached a value of tension of 0.53 MPa. The mechanical properties and in particular the higher damping behaviour of LCN-NH$_2$75 could be one explanation for the resistance to higher light power that generates rapidly higher tensions. The actuation behaviour of LCNs was compared with an acrylate side-chain LCN (LCN-acrylate) synthesized by photopolymerization by us in previous studies[43,67] and adopted here as a benchmark. Indeed, LCN-SH50 was able to slightly overcome the efficiency of LCN-acrylate (with a similar value of maximum force obtained at lower light power, Fig. S5, ESI†).

LCN-SH50 also exhibits actuation kinetic considerably higher than the other LCNs (0.82 MPa s^{-1} at 4.7 mW mm^{-2}). Despite the lower tension developed, LCN-SH75 exhibits a slightly higher rate of actuation (0.38 MPa s^{-1}) if compared with the amine-based materials (for both LCN-NH$_2$75 and LCN-NH$_2$50 equal to 0.28 MPa s^{-1}) (Fig. 4d).

Given the higher performance achieved by LCN-SH50, this material was used to conduct further light actuation experiments at higher pulse frequencies to demonstrate the rapidity of the material's response. In these experiments, a light intensity of 4.7 mW mm^{-2} was used by illuminating the sample at a frequency of 1 Hz and an illumination time of 250 ms (shown in Fig. S6, ESI†). Analysing the traces, the tension did not reach a plateau in such short intervals, yet it is evident that the material was perfectly able to follow the light pulse without hysteresis phenomena over several illumination cycles.

The thiol-based LCNs therefore present a higher level of order and a better response, both under thermal and light actuation, than the amino-based materials. If a correlation between cross-linking density and contraction in free standing thermal experiments is evident, under isometric conditions there was not an evident and clear correlation between the structure properties of the LCNs and the performances in terms of tension developed under thermal activation.

Conclusions

In this work, two classes of photoresponsive LCNs were obtained and investigated. The first one, namely the LCN-SHx series, was obtained by a one-pot thiol–acrylate photopolymerization, while

the second one, the LCN-NH$_2x$ series, was prepared in two steps through a Michael addition mediated oligomerization followed by a photo-curing step. Free-standing thermal actuation tests highlight that LCN-SHx reached higher contractions probably by virtue of their higher order parameter, while the temperature of maximum actuation was mostly controlled by the crosslinking density. The tension developed under thermal or light stimulus was not easily correlated with the structural properties of the materials, however, the experimental data highlighted that LCN-SH50 was the most efficient material being able to develop 0.95 MPa at 135 °C and, under illumination, 0.47 MPa at 4.7 mW mm^{-2}. These performances are also combined with a good resistance to many activation cycles showing an interesting profile for the development of soft actuators. Both the synthetic approaches investigated have been shown to be efficient in the preparation of thermal and light-driven LCN materials. However, for the greatest simplicity and the best performance of the products obtained, the one-step click thiol–acrylate reaction proved to be the best synthetic strategy. Also comparing these materials with the side-chain LCN produced by photopolymerization, we can conclude that the thiol–acrylate material allows higher deformation (under thermal stimuli), at the same time maintaining a similar level of tension developed by light irradiation (Fig. S5, ESI†). Since integration of the presented materials should be easily envisioned with photolithographic techniques to obtain 3D smart microstructures, these LCNs would represent a good opportunity to improve the performances needed for tunable photonic devices, micro-robots or elements of microfluidic devices. A study with a wider range of chain extenders will be of great interest in the future to understand their role in implementing the material mechanical properties and performance as actuators.

Author contributions

Conceptualization, D. M., C. P.; funding acquisition, C. P.; investigation, M. T, N. C. and N. F.; methodology, M. T, N. C., N. F and D. M.; data curation, M. T. and N. C.; resources, C. P.; supervision, D. M. and C. P.; writing – original draft, M. T.; writing – review and editing, D. M. and C. P. All authors have read and agreed to the published version of the manuscript.

Data availability

The data supporting this article have been included as part of the ESI.†

Conflicts of interest

There are no conflicts to declare.

Acknowledgements

References

1 E. Acome, S. K. Mitchell, T. G. Morrissey, M. B. Emmett, C. Benjamin, M. King, M. Radakovitz and C. Keplinger, *Science*, 2018, **359**, 61–65.

2 D. Jiao, Q. L. Zhu, C. Y. Li, Q. Zheng and Z. L. Wu, *Acc. Chem. Res.*, 2022, **55**, 1533–1545.

3 G. Vitale, B. Grandinetti, S. Querceto, D. Martella, C. Tesi, C. Poggesi, E. Cerbai, D. S. Wiersma, C. Parmeggiani, C. Ferrantini and L. Sacconi, *Macromol. Mater. Eng.*, 2022, **307**, 2200187.

4 M. Li, A. Pal, A. Aghakhani, A. Pena-Francesch and M. Sitti, *Nat. Rev. Mater.*, 2021, **7**, 235–249.

5 C. Armanini, K. Junge, P. H. Johnson, C. Whitfield, F. Renda, M. Calisti and J. Hughes, *Bioinspiration Biomimetics*, 2024, **19**, 021002.

6 H. Finkelmann, H. Kock and G. Rehage, *Makromol. Chem., Rapid Commun.*, 1981, **2**, 317–322.

7 D. Martella, D. Antonioli, S. Nocentini, D. S. Wiersma, G. Galli, M. Laus and C. Parmeggiani, *RSC Adv.*, 2017, **7**, 19940–19947.

8 S. Wang, S. Li, W. Zhao, Y. Zhou, L. Wang, J. Aizenberg and P. Zhu, *Lab Chip*, 2024, **24**, 4073–4084.

9 M. Bobnar, N. Derets, S. Umerova, V. Domenici, N. Novak, M. Lavrič, G. Cordoyiannis, B. Zalar and A. Rešetič, *Nat. Commun.*, 2023, **14**, 764.

10 B. Ni, G. Liu, M. Zhang, M. Tatoulian, P. Keller and M.-H. Li, *ACS Appl. Mater. Interfaces*, 2021, **13**, 54439–54446.

11 L. Li, X. Dong, M. Li, Y. Jiang, J. Xu, Q. Li, N. Yuan and J. Ding, *Sens. Actuators, A*, 2023, **349**, 114069.

12 S. J. D. Lugger, T. A. P. Engels, R. Cardinaels, T. Bus, D. J. Mulder and A. P. H. J. Schenning, *Adv. Funct. Mater.*, 2023, **33**, 2306853.

13 J. M. Boothby, H. Kim and T. H. Ware, *Sens. Actuators, B*, 2017, **240**, 511–518.

14 K. Kim, Y. Guo, J. Bae, S. Choi, H. Y. Song, S. Park, K. Hyun and S. Ahn, *Small*, 2021, **17**, 2100910.

15 C. Feng, C. P. H. Rajapaksha, J. M. Cedillo, C. Piedrahita, J. Cao, V. Kaphle, B. Lüssem, T. Kyu and A. Jákli, *Macromol. Rapid Commun.*, 2019, **40**, 1900299.

16 H. Guo, A. Priimagi and H. Zeng, *Adv. Funct. Mater.*, 2022, **32**, 2108919.

17 O. M. Wani, H. Zeng and A. Priimagi, *Nat. Commun.*, 2017, **8**, 15546.

18 Y. Gao, X. Wang and Y. Chen, *RSC Adv.*, 2024, **14**, 14278–14288.

19 H. Finkelmann, A. Greve and M. Warner, *Eur. Phys. J. E:Soft Matter Biol. Phys.*, 2001, **5**, 281–293.

20 T. J. White and D. J. Broer, *Nat. Mater.*, 2015, **14**, 1087–1098.

21 B. R. Donovan, V. M. Matavulj, S. Ahn, T. Guin and T. J. White, *Adv. Mater.*, 2019, **31**, 1805750.

22 H. Zeng, O. M. Wani, P. Wasylczyk, R. Kaczmarek and A. Priimagi, *Adv. Mater.*, 2017, **29**, 1701814.

23 H. Guo, H. Zeng and A. Priimagi, *Multifunct. Mater.*, 2022, **5**, 024001.

24 M. Wang, Z.-W. Cheng, B. Zuo, X.-M. Chen, S. Huang and H. Yang, *ACS Macro Lett.*, 2020, **9**, 860–865.

25 H. Zeng, C. Parmeggiani, D. Martella, P. Wasylczyk, M. Burresi and D. S. Wiersma, ed. G. Von Freymann, W. V. Schoenfeld and R. C. Rumpf, 2016, 97590Y.

26 M. Rogóż, Z. Dziekan, K. Dradrach, M. Zmyślony, P. Nałęcz-Jawecki, P. Grabowski, B. Fabjanowicz, M. Podgórska, A. Kudzia and P. Wasylczyk, *Materials*, 2022, **15**, 8214.

27 M. Camacho-Lopez, H. Finkelmann, P. Palffy-Muhoray and M. Shelley, *Nat. Mater.*, 2004, **3**, 307–310.

28 P. Sartori, R. S. Yadav, J. Del Barrio, A. DeSimone and C. Sánchez-Somolinos, *Adv. Sci.*, 2024, **11**, 2308561.

29 K. Liu, F. Hacker and C. Daraio, *Sci. Rob.*, 2021, **6**, eabf5116.

30 P. Lyu, M. O. Astam, C. Sánchez-Somolinos and D. Liu, *Adv. Int. Syst.*, 2022, **4**, 2200280.

31 Q. Yang, C. Peng, J. Ren, W. Zhao, W. Zheng, C. Zhang, Y. Hu and X. Zhang, *Adv. Opt. Mater.*, 2019, **7**, 1900784.

32 S. Serak, N. Tabiryan, R. Vergara, T. J. White, R. A. Vaia and T. J. Bunning, *Soft Matter*, 2010, **6**, 779–783.

33 Z. Deng, K. Li, A. Priimagi and H. Zeng, *Nat. Mater.*, 2024, **23**, 1728.

34 I. De Bellis, D. Martella, C. Parmeggiani, D. S. Wiersma and S. Nocentini, *Adv. Funct. Mater.*, 2023, **33**, 2213162.

35 S. Woska, A. Münchinger, D. Beutel, E. Blasco, J. Hessenauer, O. Karayel, P. Rietz, S. Pfleging, R. Oberle, C. Rockstuhl, M. Wegener and H. Kalt, *Opt. Mater. Express*, 2020, **10**, 2928.

36 M. Fallah-Darrehchi, P. Zahedi, P. Harirchi and M. Abdouss, *ACS Appl. Polym. Mater.*, 2023, **5**, 1076–1091.

37 D. Martella, M. Mannelli, R. Squecco, R. Garella, E. Idrizaj, D. Antonioli, M. Laus, D. S. Wiersma, T. Gamberi, P. Paoli, C. Parmeggiani and T. Fiaschi, *iScience*, 2021, **24**, 103077.

38 S. H. Choi, J. H. Kim, J. Ahn, T. Kim, Y. Jung, D. Won, J. Bang, K. R. Pyun, S. Jeong, H. Kim, Y. G. Kim and S. H. Ko, *Nat. Mater.*, 2024, **23**, 834–843.

39 J. Koo, M. Kim, J. Hyeong, D. Yu, S. Kim, J. Jang, M. Oh, Y. Wi, H. Ko and K. Jeong, *Adv. Opt. Mater.*, 2023, **11**, 2300844.

40 A. R. Tajbakhsh and E. M. Terentjev, *Eur. Phys. J. E:Soft Matter Biol. Phys.*, 2001, **6**, 181–188.

41 G. H. F. Bergmann, H. Finkelmann, V. Percec and M. Zhao, *Macromol. Rapid Commun.*, 1997, **18**, 353–360.

42 H.-F. Lu, M. Wang, X.-M. Chen, B.-P. Lin and H. Yang, *J. Am. Chem. Soc.*, 2019, **141**, 14364–14369.

43 S. Donato, D. Martella, M. Salzano De Luna, G. Arecchi, S. Querceto, C. Ferrantini, L. Sacconi, P. Brient, C. Chatard, A. Graillot, D. S. Wiersma and C. Parmeggiani, *Macromol. Rapid Commun.*, 2023, **44**, 2200958.

44 D. Ditter, P. Blümler, B. Klöckner, J. Hilgert and R. Zentel, *Adv. Funct. Mater.*, 2019, **29**, 1902454.

45 S. Donato, S. Nocentini, D. Martella, S. Kolagatla, D. S. Wiersma, C. Parmeggiani, C. Delaney and L. Florea, *Small*, 2024, **20**, 2306802.

46 H. Tian, Z. Wang, Y. Chen, J. Shao, T. Gao and S. Cai, *ACS Appl. Mater. Interfaces*, 2018, **10**, 8307–8316.

47 G. Barrera, D. Martella, F. Celegato, N. Fuochi, M. Coïsson, C. Parmeggiani, D. S. Wiersma and P. Tiberto, *Adv. Sci.*, 2024, 2408273.

48 H. Kim, J. A. Lee, C. P. Ambulo, H. B. Lee, S. H. Kim, V. V. Naik, C. S. Haines, A. E. Aliev, R. Ovalle-Robles, R. H. Baughman and T. H. Ware, *Adv. Funct. Mater.*, 2019, **29**, 1905063.

49 M. R. Vinciguerra, D. K. Patel, W. Zu, M. Tavakoli, C. Majidi and L. Yao, *ACS Appl. Mater. Interfaces*, 2023, **15**, 24777–24787.

50 V. Cresta, G. Romano, A. Kolpak, B. Zalar and V. Domenici, *Polymers*, 2018, **10**, 773.

51 Y. Li, T. Liu, V. Ambrogi, O. Rios, M. Xia, W. He and Z. Yang, *ACS Appl. Mater. Interfaces*, 2022, **14**, 14842–14858.

52 T. H. Ware, Z. P. Perry, C. M. Middleton, S. T. Iacono and T. J. White, *ACS Macro Lett.*, 2015, **4**, 942–946.

53 H. Yang, A. Buguin, J.-M. Taulemesse, K. Kaneko, S. Méry, A. Bergeret and P. Keller, *J. Am. Chem. Soc.*, 2009, **131**, 15000–15004.

54 D. Martella, C. Parmeggiani, D. S. Wiersma, M. Piñol and L. Oriol, *J. Mater. Chem. C*, 2015, **3**, 9003–9010.

55 F. Lupi, D. Martella, S. Nocentini, D. Antonioli, M. Laus, D. S. Wiersma and C. Parmeggiani, *ACS Appl. Polym. Mater.*, 2021, **3**, 1602–1609.

56 T. S. Hebner, H. E. Fowler, K. M. Herbert, N. P. Skillin, C. N. Bowman and T. J. White, *Macromolecules*, 2021, **54**, 11074–11082.

57 N. P. Godman, B. A. Kowalski, A. D. Auguste, H. Koerner and T. J. White, *ACS Macro Lett.*, 2017, **6**, 1290–1295.

58 D. T. Kennedy, J. D. Hoang, M. F. Toney and T. J. White, *Macromolecules*, 2024, **57**, 10032–10040.

59 H.-H. Yoon, D.-Y. Kim, K.-U. Jeong and S. Ahn, *Macromolecules*, 2018, **51**, 1141–1149.

60 L. Halbardier, E. Goldbach, C. Croutxé-Barghorn, A.-S. Schuller and X. Allonas, *RSC Adv.*, 2022, **12**, 30381–30385.

61 W. Zou, X. Lin and E. M. Terentjev, *Adv. Mater.*, 2021, **33**, 2101955.

62 K. M. Lee, H. Koerner, R. A. Vaia, T. J. Bunning and T. J. White, *Macromolecules*, 2010, **43**, 8185–8190.

63 G. E. Bauman, J. M. McCracken and T. J. White, *Angew. Chem., Int. Ed.*, 2022, **61**, e202202577.

64 M. Barnes, S. Cetinkaya, A. Ajnsztajn and R. Verduzco, *Soft Matter*, 2022, **18**, 5074–5081.

65 B. Lei, Z.-Y. Wen, H.-K. Wang, J. Gao and L.-J. Chen, *ACS Appl. Mater. Interfaces*, 2024, **16**, 1596–1604.

66 M. Pilz Da Cunha, E. A. J. Van Thoor, M. G. Debije, D. J. Broer and A. P. H. J. Schenning, *J. Mater. Chem. C*, 2019, **7**, 13502–13509.

67 C. Ferrantini, J. M. Pioner, D. Martella, R. Coppini, N. Piroddi, P. Paoli, M. Calamai, F. S. Pavone, D. S. Wiersma, C. Tesi, E. Cerbai, C. Poggesi, L. Sacconi and C. Parmeggiani, *Circ. Res.*, 2019, **124**, e44–e54.